Rheologica Acta
© Springer-Verlag 2005
DOI 10.1007/s00397-005-0449-0

Original Contribution

Fluid dynamics analysis of channel flow geometries for materials characterization in microfluidic devices

Frederick R. Phelan Jr (✉) · Steven D. Hudson · Matthew D. Handler

F. R. Phelan Jr · S. D. Hudson · M. D. Handler
Polymers Division, NIST, 100 Bureau Dr., STOP 8542, Gaithersburg, MD 20899, USA

✉ F. R. Phelan Jr
Phone: +1-(301)-9756761
Fax: +1-(301)-9754924
E-mail: frederick.phelan@nist.gov

Received: 20 January 2004 / **Accepted:** 7 February 2005

Abstract The fluid dynamics of geometries for liquid state materials characterization in microfluidic devices are investigated. Numerical simulation together with flow classification criteria are used to explore combinations of geometry and boundary conditions for which the flow type can be adjusted between simple shear and extension, while providing adequate flow strength and a stable environment for material observation. Two classes of flow geometries are identified. Both make use of opposing, laterally offset fluid streams that produce a stagnation point in the center of the geometry. In the first class, the flow type is manipulated by changing parameters inherent to the base geometry. This first case serves as a basis for identifying a second class in which the flow type is manipulated by changing the pressure boundary conditions, while keeping the geometry constant.

Electronic Supplementary Material is available for this article if you access the article at http://dx.doi.org/10.1007/s00397-005-0449-0.

Keywords Microfluidics · Nano-materials · Flow classification · Four roll mill · Finite element simulation

---

Introduction

Fluid flow in microfluidic devices is becoming more and more common, driven by the miniaturization of many technologies (Ouellette 2003; Thorsen et al. 2002; Ceriotti et al. 2003; Chow 2002; Hasselbrink et al. 2002). With the continued emergence of nano-materials, and nanoliter volume processing, the development of microfluidic devices for the characterization of process induced material properties appears to be a natural blending of two important technologies. Such devices would afford a number of advantages over conventional methods, including greater speed, replacement of multiple manual steps, conservation of expensive and/or limited quantity reagents and chemicals, access to a wider array of detection methods, and reduced human error. We seek to apply microfluidics technology to the measurement of material properties, specifically, to develop a microfluidic device for liquid state materials characterization. A variety of applications for such a platform can be anticipated ranging from such traditional areas as interfacial dynamics, viscosity measurement, molecular stretching and crystallization, to newer areas such as dispersion/aggregation of nanoparticle fillers, and flow induced changes in biological cells.

The ideal types of flow for the characterization of fluids are linear flows which are described by the stream function, ψ, and corresponding velocity vector, $\underline{V}$

$$\psi = \frac{1}{2}\left(\xi\phi x^2 - \phi y^2\right), \tag{1}$$

$$\underline{v} = (\phi y, \xi\phi x). \tag{2}$$

The nature of these kinematics are characterized by the constants ξ and φ . The quantity ξ is the flow type, and indicates the nature of the deformation experience by the fluid; the flow is extensional for ξ=1, shear for ξ=0, and pure rigid body rotation for ξ =−1. The quantity φ is the flow strength, and indicates the magnitude of the velocity gradient relative to the flow type. In simple shear, it is equivalent to the shear rate. In classifying flows (Astarita 1979; Thompson and Mendes 2004), the flow type is often thought of as the primary criterion because fluid response changes in fundamental way as this quantity varies. The flow strength constitutes a second type of flow classification criterion because many fluids experience a critical response after threshold

value of flow strength is reached [e.g., chain extension in dilute polymer solutions (De Gennes 1974); drop breakup in emulsions (Taylor 1934)]. Thus, the ability to control flow type, and achieve adequate flow strength are extremely important goals in developing a flow device for liquid state materials characterization.

Linear flows have the desirable property that the velocity gradient tensor is homogeneous (constant throughout the flow) and the flow type is uniform, making measurement of flow properties as a function of deformation type and deformation rate unambiguous. Another important property of linear flows is that they contain a stagnation point at the origin, $\underline{x} = (0,0)$. The stagnation point serves a number of useful purposes in the present context. First, the material residence time in the neighborhood of the stagnation point is high, giving the material adequate time to respond to the applied deformation. Residence time is in effect, a third type of flow classification criterion (Astarita 1979). In addition, the long residence time also provides a stable environment for material observation and measurement, and it allows one to ignore the inhomogeneities present in a complex flow, provided that the stagnation region is reasonably broad, and the flow gradients are suitably uniform.

A number of devices that approximate particular modes of linear flows at the macroscale are available. Devices used mainly for extensional or mixed extensional/shear flow include the four roll mill (Bentley and Leal 1986a, b; Fuller and Leal 1981; Taylor 1934), two roll mill (Frank and Mackley 1976; Hills 2002; Lee et al. 2002; Price et al. 2003; Remmelgas and Leal 2000; Reyes and Geffroy 2000a, 2000b; Singh and Leal 1996), six roll mill (Berry and Mackley 1977), and cross-slot geometry (Chow et al. 1988; Keller and Odell 1985). Viscometric devices such as the cone and plate, parallel plate and Couette flow geometries (Bird et al. 1982) produce simple shear. However, none of these avail themselves particularly to our present investigation in the sense that in the context microfluidics, it is desirable to have a single device which produces the full range of kinematics available in linear flows, which none of them is able to do. The device that comes closest to the desired functionality is the four-roll mill. While this is primarily thought of as a device for producing planar extension (ξ=1.0), it can also be used to provide mixed flows in the range $0.2<\xi<1$ (Bentley and Leal 1986a, b), and rotational flows where $\xi=-1$ (Higdon 1993). However, the four roll geometry is inadequate for generating simple shear (ξ=0), and difficulties can be anticipated in trying to produce and control a miniature device with moving parts. This leads us to seek a solution based on channel flow.

In this study, a pressure driven device using microchannels is sought that has an adjustable flow type, approximating the function of the four-roll mill. In particular, we investigate classes of channel flows in which the full range of linear flows can be approximated in the neighborhood surrounding a stagnation point. To evaluate various candidate geometries, finite element flow simulations in the zero Reynolds number limit were undertaken. The FEM solutions were analyzed using classification criteria to determine combinations of geometry and boundary conditions for which the flow type can be adjusted between simple shear and extension in the neighborhood surrounding the stagnation point, while at the same time providing adequate flow strength.

Two classes of flow geometries are identified. Both make use of opposing, laterally offset fluid streams, which produce a stagnation point. The use of opposing streams enables the generation of a stagnation point. While this is normally a means to generate pure extension, the lateral offset which is also employed introduces vorticity at the stagnation point, enabling the generation of shear and even rotation. In the first geometry class, the flow type can be manipulated by changing parameters inherent to the base geometry. This first case serves as a baseline for identifying a second class of geometries in which the flow type can be manipulated by varying the pressure boundary conditions while keeping the geometry constant. This latter case is probably the more useful not only in terms of construction, but for linking the device with a computer control system for placement and manipulation of a second phase at the stagnation point.

Modeling

Flow simulation

To evaluate various candidate geometries, flow generated in these devices was simulated using the finite element method. All flows were assumed to be steady, two-dimensional and at the zero Reynolds number limit. Modeling was carried out using the commercial finite element packages [1] FIDAP (2003a) and FlexPDE (2003b).

The governing equations solved by FIDAP are the Navier-Stokes equations together with the incompressible condition

[1] Identification of a commercial product is made only to facilitate reproducibility and to adequately describe procedure. In no case does it imply endorsement by NIST or imply that it is necessarily the best product for the procedure

$$\rho \underline{v} \cdot \nabla \underline{v} = -\nabla p + \eta \nabla^2 \underline{v}, \tag{3}$$

$$\nabla \cdot \underline{v} = 0. \tag{4}$$

FlexPDE makes use of the alternative incompressible formulation

$$\nabla^2 p = -\nabla \cdot \nabla \cdot \left(\rho \underline{v} \underline{v} \right) + \beta (\nabla \cdot \underline{v}), \tag{5}$$

where β is a large value chosen such that $\nabla \cdot \underline{v}$ is sufficiently minimized.

Flow classification in non-homogeneous flows

The uniform nature of linear flows makes measurement of flow properties as a function of deformation rate unambiguous. However, in the types of channel geometries inherent to microfluidic devices, linear flows are not perfectly achievable and we seek to approximate linear flows in the neighborhood of a stagnation point to achieve the desired flow kinematics. Therefore, generalized flow classification criteria for discerning the flow type as a function of position in non-homogeneous flows are a useful tool for determining the utility of various complex flow fields for producing a correct flow type in a region surrounding a stagnation point.

A suitable objective criterion for classifying the flow type in complex flows has been developed by Astarita (1979). The type of a flow may be determined by computing the non-dimensional number

$$\Xi = \frac{\underline{\underline{D}} : \underline{\underline{D}} + \underline{\underline{W}} : \underline{\underline{W}}}{\underline{\underline{D}} : \underline{\underline{D}} - \underline{\underline{W}} : \underline{\underline{W}}}, \tag{6}$$

where $\underline{\underline{D}}$ is the stretching tensor given by

$$\underline{\underline{D}} = \frac{1}{2} \left(\nabla \underline{v} + \nabla \underline{v}^{\mathrm{T}} \right), \tag{7}$$

and $\underline{\underline{W}}$ is the a tensor defined as

$$\underline{\underline{W}} = \underline{\underline{\omega}} - \underline{\underline{\Omega}}, \tag{8}$$

where

$$\underline{\underline{\omega}} = \frac{1}{2}\left(\nabla \underline{v} - \nabla \underline{v}^{\mathrm{T}}\right), \tag{9}$$

$$\underline{\underline{\Omega}} = \frac{\mathrm{d}\underline{\underline{E}}}{\mathrm{d}t} \cdot \underline{\underline{E}}^{-1}. \tag{10}$$

In the definition of $\underline{\underline{W}}$, $\underline{\underline{\omega}}$ is the vorticity tensor, $\underline{\underline{E}}$ is the matrix of right eigenvectors of $\underline{\underline{D}}$, and the tensor $\underline{\underline{\omega}}$ describes the rate of rotation of the principal axes of $\underline{\underline{D}}$. The tensor $\underline{\underline{W}}$ is therefore the difference between the rate of rotation of a fluid element and the rate of rotation of the principal axes of stretch. Like the constant ξ in linear flows, the variable Ξ has a value equal to 1 in purely extensional flows, 0 in shear flows, and -1 in a pure rigid body rotation. Values between 1 and 0 indicate a mixture of extension and shear, and values between 0 and -1 indicate mixed shear and rotation. If the linear flow kinematics given by Eq. 2 are used in Eq. 6, one finds that Ξ and the linear flow type ξ are simply related by the expression, $\Xi = 2\xi/\left(\xi^2 + 1\right)$, with the inverse relationship being $\xi = \Xi/\left(1 + \sqrt{1 - \Xi^2}\right)$, over the bounds $-1 \leqslant \Xi \leqslant 1$

For steady 2-D flows, the stretching and vorticity tensors can be generalized as

$$\underline{\underline{D}} = \begin{bmatrix} \varepsilon & \gamma \\ \gamma & -\varepsilon \end{bmatrix}, \tag{11}$$

$$\underline{\underline{\omega}} = \begin{bmatrix} 0 & \omega \\ -\omega & 0 \end{bmatrix}, \tag{12}$$

and $\underline{\underline{\Omega}}$ and $\underline{\underline{W}}$ take on the anti-symmetric forms

$$\underline{\underline{\Omega}} = \begin{bmatrix} 0 & \Omega \\ -\Omega & 0 \end{bmatrix}, \tag{13}$$

$$\underline{\underline{W}} = \begin{bmatrix} 0 & W \\ -W & 0 \end{bmatrix}, \tag{14}$$

where $W = \omega - \Omega$ and

$$\Omega = \frac{\gamma\left(u\frac{\partial \varepsilon}{\partial x} + v\frac{\partial \varepsilon}{\partial y}\right) - \varepsilon\left(u\frac{\partial \gamma}{\partial x} + v\frac{\partial \gamma}{\partial y}\right)}{2\sqrt{\varepsilon^2 + \gamma^2}}. \tag{15}$$

In this case, Ξ is given by the expression

$$\Xi = \frac{\varepsilon^2 + \gamma^2 - W^2}{\varepsilon^2 + \gamma^2 + W^2}. \tag{16}$$

Eq. 16 was used in this study to classify the flow type of the kinematics computed from FEM simulation. In FIDAP, the value of Ξ was evaluated by means of a user defined FORTRAN subroutine, while in FlexPDE, it was evaluated using the scripting language inherent to the package.

For classifying flow strength, there are a number of possible criteria, based upon what one seeks to measure. A persistent strain rate as derived from the flow classification scheme given in Astarita (1979) is

$$\varepsilon_{\mathrm{p}} = \sqrt{\varepsilon^2 + \gamma^2 - W^2}. \tag{17}$$

This rate is based on the difference between the stretch rate of material element and the rate of rotation with respect to the principal axes of the material element, and is useful for determining whether a flow is "weak" or "strong‘', e.g., (Astarita 1979; Chella and Ottino 1985; Huilgol 1980; Tanner 1976). One problem with this criterion is that it becomes imaginary in regions of the flow where $-1 < \Xi < 0$ In addition, in the present case we are more interested in simply comparing the relative magnitude of the deformation at different points in the flow as a smeans for discriminating between various combinations of geometry and boundary conditions, rather than determining whether a flow is "weak" or "strong" in a material sense.

An objective measure, useful for comparing the relative strength of different flow fields is the maximum eigenvalue of the stretching tensor given by

$$\lambda = \sqrt{\varepsilon^2 + \gamma^2}, \tag{18}$$

which is equivalent to $\sqrt{\frac{1}{2}tr\underline{\underline{D}}^2}$ or $(1+\xi)\,\phi$ in terms of the linear flow kinematics given in Eq. 2. Based on this, a relative flow strength can be defined as

$$S_{\mathrm{r}} = \frac{\lambda}{\lambda_{\mathrm{ref}}}, \tag{19}$$

where λ_{ref} is the flow strength at some reference point in the flow field. In what follows, we classify the flow strength in different flow fields using Eq. 19. The reference flow strength is usually taken to be an average flow strength at the inlet or outlet of a channel geometry. This enables comparison

of the strength of deformation in the stagnation region with the deformation in the pressure driven channels that drive the flow.

Geometry class 1: manipulation of flow type using geometric asymmetry

In determining the parameters of a flow device that could be used to generate a range of approximately linear flows in the region surrounding a stagnation point, it was recognized that creating a flow with a stagnation point requires the use of opposing fluid streams. While this is generally a means to produce extensional flow, as discussed above, by creating lateral offset, or asymmetry, between the opposing streams, vorticity is generated allowing shear and even rotation to be produced as well. We make use of this principle in our investigation. In this section, we consider first the case of an asymmetric cross cell (Fig. 1), which illustrates the principle of lateral offset for producing vorticity. A second geometry based on parallel, laterally offset fluid streams is then introduced (Fig. 5). This geometry displays all the flow type features of the asymmetric cross cell, but has much better all around flow properties.

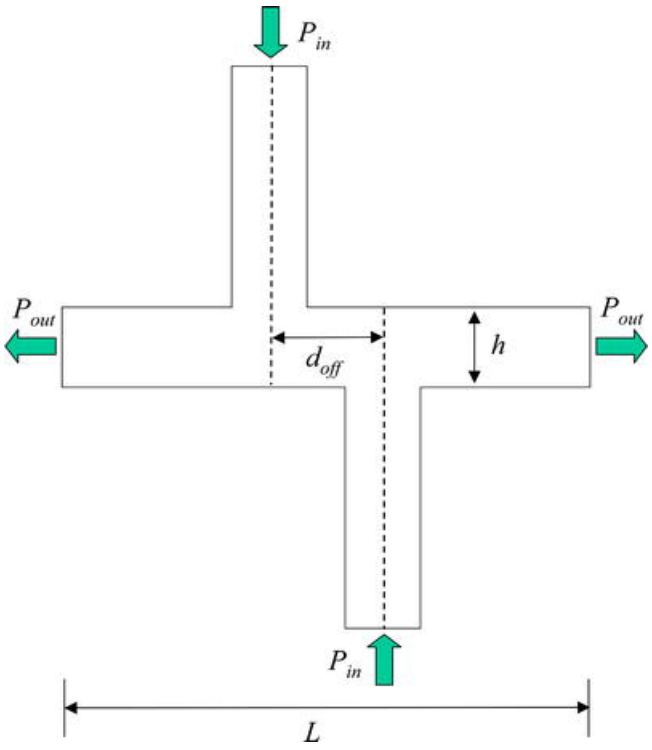

Fig. 1 Geometry, parameters and boundary condition for the asymmetric cross flow cell

Asymmetric cross flow cell

The geometry under consideration is shown in Fig. 1. It consists of a cross flow channel, parameterized by an offset distance, d_{off}

Flow enters the system through the vertical channels, and exits through the horizontal. A constant, positive pressure boundary condition is imposed on the entrances, and a pressure of zero is imposed on the outlet streams. The geometric parameters and boundary conditions used in the calculations are summarized in Table 1.

[Table 1 will appear here. See end of document.]

Streamlines in the stagnation flow region for offset distances of 0, 1.3, 1.5 and 2, are shown in Figures 2a-d. Fig. 2a shows the well known result of approximate planar extension for an offset distance of zero. However, the accompanying plots show that as the offset distance increases, the incoming streams undergo an increasingly asymmetric split, causing the material to tend to exit out of one side or the other. The resulting flow fields become increasingly shear like, and finally fully rotational, as illustrated in Fig. 2b-d.

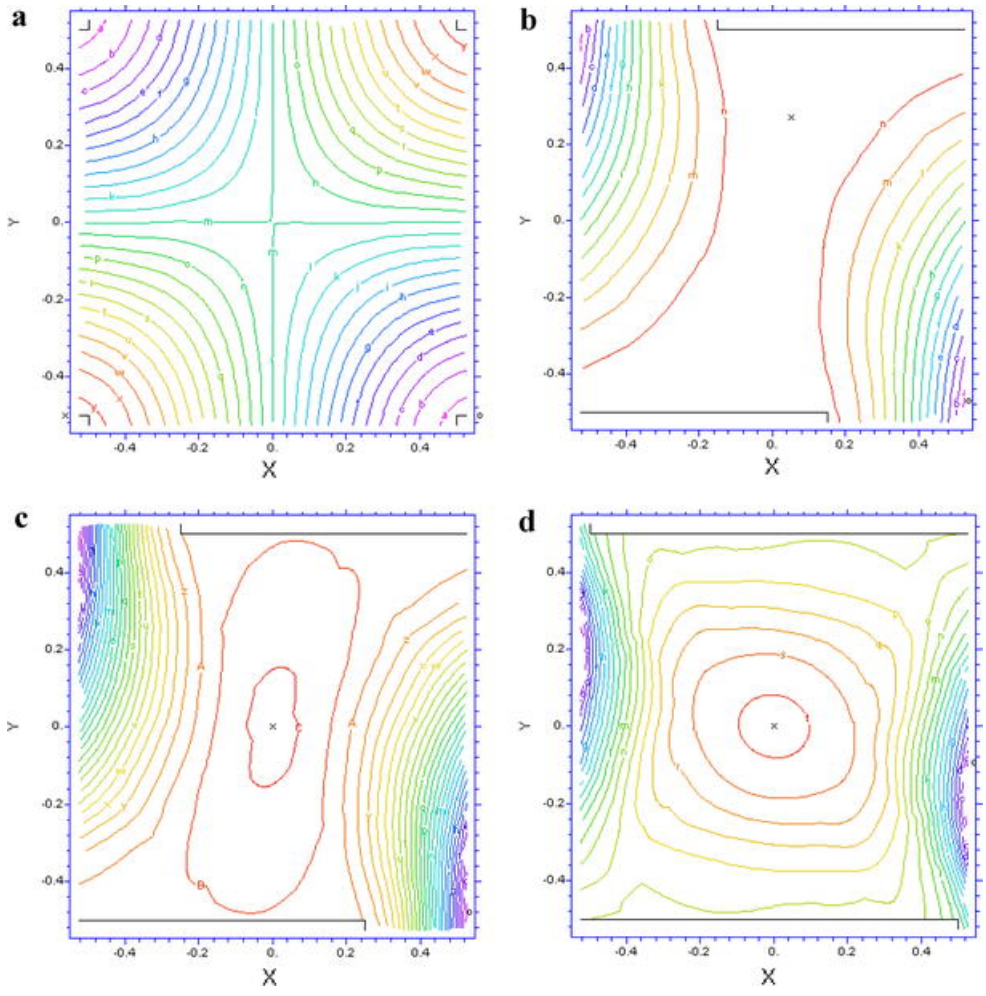

Fig. 2 Streamlines in the stagnation region for the asymmetric cross flow cell for different offset distances. **a** Extensional behavior for d_{off}=0 **b** Increased shear like behavior for d_{off}=1.3 **c** A shear flow type of approximately zero for d_{off}=1.5 **d** Full rotational flow for d_{off}=2

Plots of flow type and relative flow strength at the stagnation point, as a function of d_{off} are shown in Figures 3–4. The value for relative flow strength is defined with respect to the integral average flow strength at the inlet. The flow type plot confirms the qualitative observation noted in the streamline contours. The flow type is basically unity for an offset distance of zero. This value gradually decreases as the offset increases, passing through zero (shear) at approximately d_{off}=1.5, and is very close to −1 (pure rotation) at the maximum calculated value of d_{off}=2.

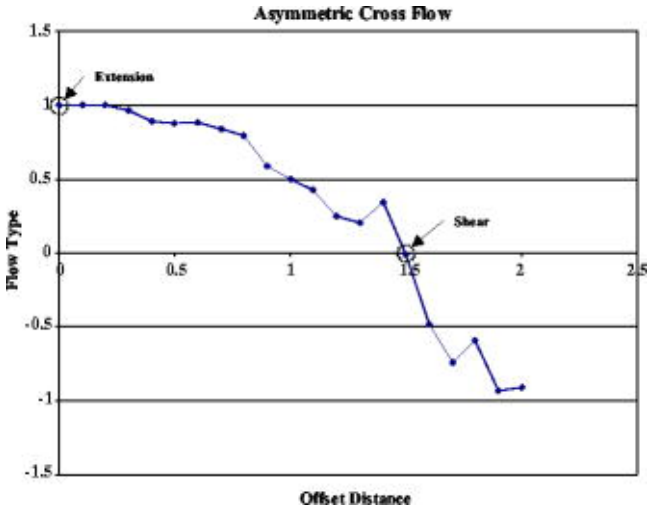

Fig. 3 Flow type (Ξ) as a function of offset distance for the asymmetric cross flow cell

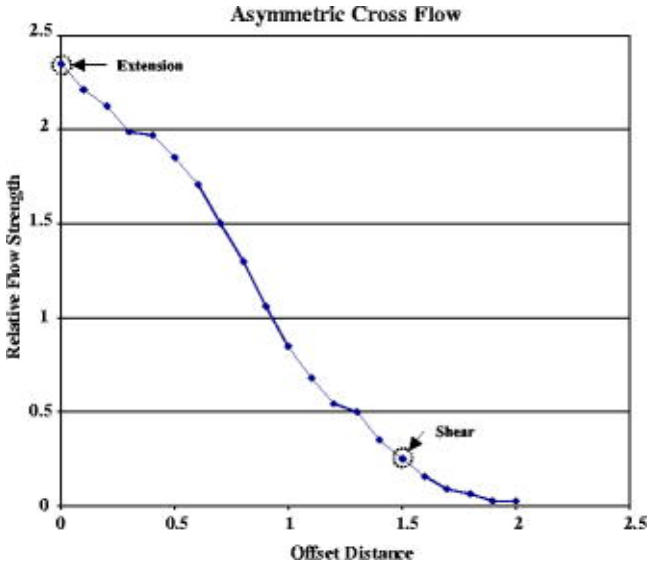

Fig. 4 Relative flow strength (S_r) as a function of offset distance for the asymmetric cross flow cell

The relative flow strength decreases as the offset increases, from a value of approximately 2.2 for the extensional flow case, to near zero for the case of pure rotation. The shear value is approximately 0.3, indicating that the deformation remains a fairly generous portion of the average inlet flow strength for this case. Exact values for flow type and relative flow strength at the stagnation point for these respective cases are listed in Table 2.

[Table 2 will appear here. See end of document.]

Parallel, laterally offset channels

The results for the asymmetric cross flow illustrate the principle of using asymmetry to generate shear and rotational type flows at a stagnation point. The geometry of parallel, laterally offset channels, which also makes use of this principle, is shown in Fig. 5. Fluid enters from a channel on each side whose width is h, and impinges in the central region creating a stagnation point in the center. The fluid exits through channels of width H, that are aligned parallel with the incoming streams. The inlet and outlet streams are separated by a spacer fin of width h_{fin}. The tips of the separating fins are offset by a distance d. The nature of the geometry gives rise to a natural asymmetry between the impinging streams. Geometric parameters and boundary conditions used in the calculations are given in Table 3.

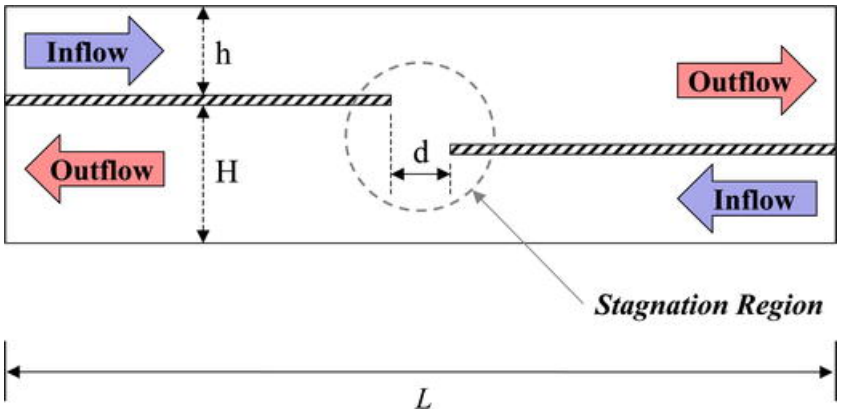

Fig. 5 Geometry, parameters and boundary condition for the parallel, laterally offset channel geometry

[Table 3 will appear here. See end of document.]

Simulation shows that the flow type observed in the stagnation region of this geometry is mainly controlled by changing the offset distance between the fin tips. This is illustrated in the streamline contours shown in Fig. 6a-c.When the offset is slightly negative (i.e., overlapping), a recirculation forms and the flow type is rotational (Fig. 6a). When the offset is large, the inlet stream splits: part of it continues straight and the other part bends around the spacer plate and exits with the outlet

stream associated with the opposing inlet stream (Fig. 6c). This "splitting" creates an extensional flow in the stagnation region. Shear flow is observed as the natural intermediary between extension and rotation (Fig. 6b). The aspect ratio *H/h* also plays a role in the flow type, but this effect is slight.

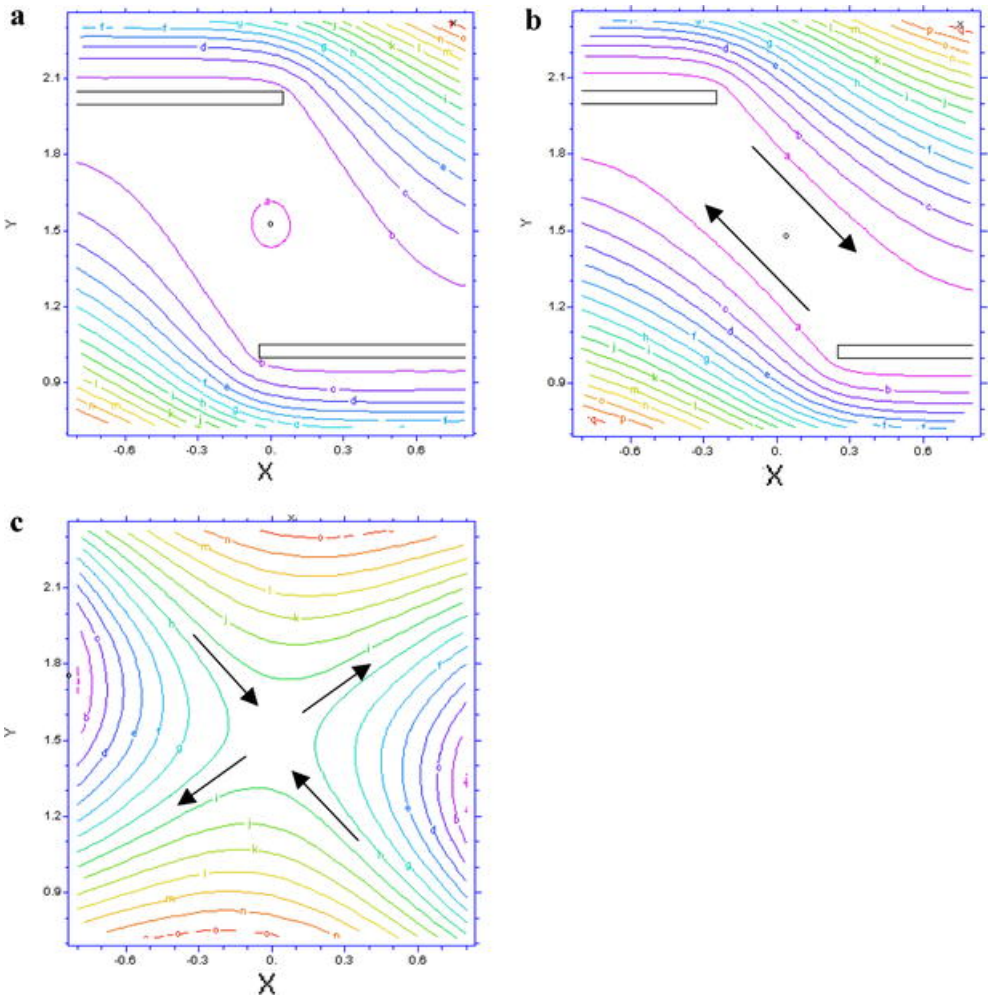

Fig. 6 Streamlines in the stagnation region for the parallel, laterally offset, channel geometry at different offset distances. **a** Rotational flow for over lapping fins. **b** Shear flow as an intermediate state at increased offset distance. **c** Extensional flow at high fin offset distances

---

Plots of flow type and relative flow strength at the stagnation point, as a function of *d* are shown in Figs. 7 and 8, for an aspect ratio of *H/h*=2.0. The flow strength is defined relative to the integral average flow strength at the outlet. In accordance with our qualitative understanding of the flow deduced from the streamlines, the flow type is approximately −1 for an offset distance of slightly less than zero, and gradually increases, passing through zero (shear) at a value of *d*=0.4, and is very close to unity (0.995) at the maximum value of *d*=3.5. The relative flow strength shown in Fig. 8 passes through a maximum. It is very low when the offset is small and the stagnation flow

kinematics are rotational. It increases with the offset distance through the shear region, but eventually drops off again as the flow type increases toward a value of unity. The shear and extensional flow strength values are approximately 0.4 and 0.45, respectively. Tabulated values for flow type and relative flow strength at the stagnation point for these respective cases are listed in Table 4.

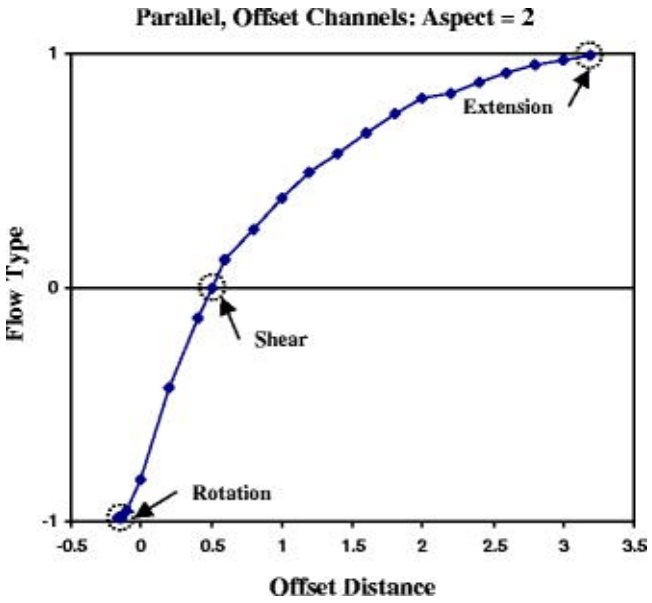

Fig. 7 Flow type (Ξ) as a function of offset distance for the parallel, laterally offset, channel geometry for $H/h = 2$. The *circled points* represent the cases of rotation, shear and extensional flow, respectively

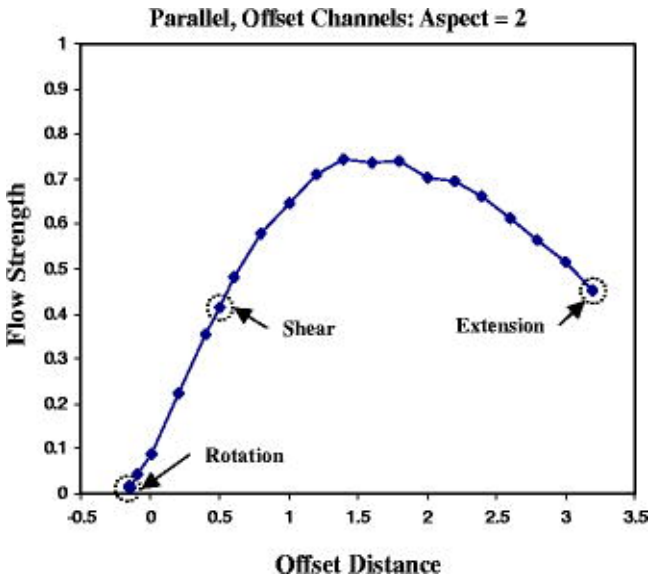

Fig. 8 Relative flow strength (S_r) as a function of offset distance for the parallel, laterally offset, channel geometry. The *circled points* represent the cases of rotation, shear and extensional flow, respectively

[Table 4 will appear here. See end of document.]

What is nearly as important as the exact value of the flow type at the stagnation point is the relative uniformity of the flow type in the stagnation region. Contour plots of the flow type for offset distances corresponding to the extensional and shear cases are shown in Fig. 9a-b. The flow type in the stagnation region is quite large and uniform for the extensional flow case. All values are within 10% of the case of pure extension over a region whose diameter is approximately equal to the vertical separation between fins in Fig. 9a.

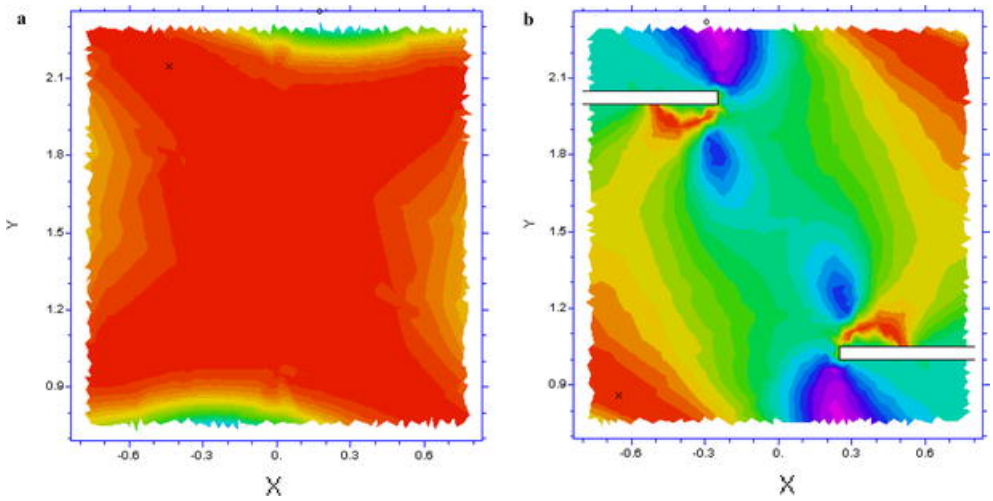

Fig. 9 Flow type (Ξ) contours in the stagnation region for the parallel, laterally offset, channel geometry for the cases of **a** extension, and **b** shear

---

The shear case depicted by the streamlines in Fig. 6b and the flow type in Fig. 9b is characterized by a highly elongated vortex. This is somewhat representative of the shear flow results found throughout. Shear appears as an intermediate state between extension and rotation. In general, the bulk of the center region has streamlines that are approximately parallel and a flow type that is near zero. However, there is a very small degree of rotation at the very tips of the vortex where the flow type is slightly negative. Thus, shear flows are an obtainable class of flows, but the radius of this zone is slightly smaller than it is for the case of extension. The degree to which the shear zone radius is reduced is somewhat geometry dependant. An important determining factor in this is the value of the flow type at the rotational tips. In the present case it is approximately −0.4.

Geometry class 2: manipulation of flow type via boundary condition

In the previous section, a class of flow geometries was introduced that enabled the approximation of a full range of linear flows in the neighborhood surrounding a stagnation point. However, the manipulation of the flow type is realized by changing the geometry. In practice, a more desirable platform is one in which the geometry is kept constant, and the flow type is manipulated through the boundary conditions that are applied as is done, for example, in the four roll mill. Such a device would be much easier to construct and control experimentally.

With this goal in mind, a second geometry class is introduced which represents a modification of the parallel, laterally offset channel geometry. The geometry together with boundary conditions are depicted in Fig. 10. For ease of reference, we shall sometimes refer to this as the "St. Brigid's Cross" geometry. The figure shows that two extra flow channels of width H_2 have been added to supply the stagnation region, in a direction normal to the existing channels. The arms are asymmetrically offset from the center of the channel on the top and bottom of the geometry by distances of $\pm H_2/2$, respectively. These additional arms can be used as either inlet or outlet streams. Their purpose is to attempt to manipulate the flow type in the stagnation region by means of the pressure boundary conditions at their ends. It will be shown that the additional flow arms allow control of the kinematics in the stagnation regionin much the same way as changing the geometry did in the previous cases studied.

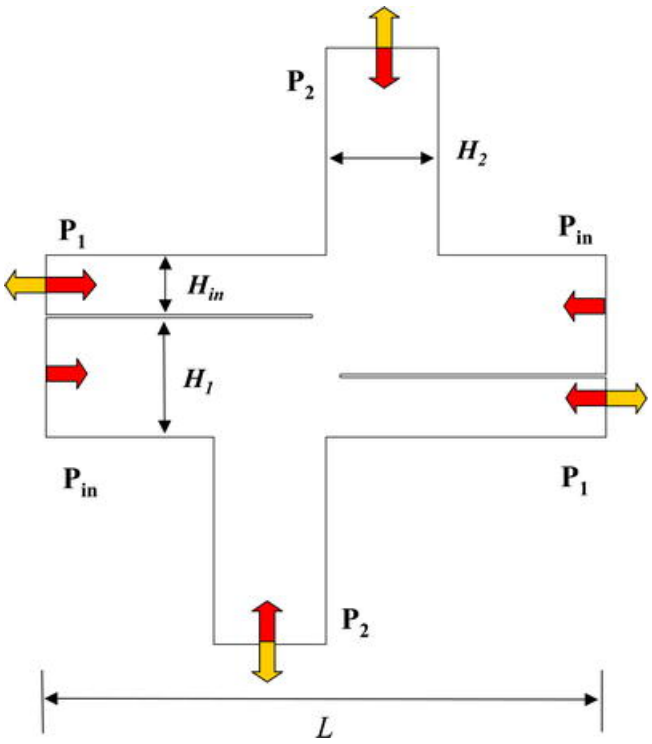

Fig. 10 Geometry, parameters and boundary condition for the parallel, laterally offset, channel geometry, with side channels ("St. Brigid's Cross" geometry)

The flow characteristics in this geometry were studied as a function of the three different boundary pressures, P_{in}, P_1, and P_2. The pressure P_{in} represents a pressure that remained fixed during a simulation, while the values of P_1 and P_2 represent pressures that were allowed to vary. The flow type at the stagnation point in this geometry turns out to be solely a function of the ratio $P_{\text{rat}} = \Delta P_1 / \Delta P_2$, where $\Delta P_1 = P_{in} - P_1$, $\Delta P_2 = P_{\text{in}} - P_2$. By specifying values for P_{in}, P_{rat} and $P_{\text{mag}} = \Delta P_2$, values for P_1, and P_2 were set as

$$P_1 = P_{\text{in}} - P_{\text{mag}} \cdot P_{\text{rat}}, \tag{20}$$

$$P_2 = P_{\text{in}} - P_{\text{mag}}. \tag{21}$$

The relevant geometric and boundary condition parameters used in the simulations to be presented are listed in Table 5.

[Table 5 will appear here. See end of document.]

Plots of flow type and relative flow strength at the stagnation point as a function of P_{rat} are shown in Fig. 11 and 12. Figure 11 shows that when the pressure ratio is highly negative the flow is rotational. As this value decreases, the amount of rotation is continually reduced and the

extensional flow type value of unity is reached at a pressure ratio of approximately −1. The streamlines for this case are depicted in Fig. 13a. As the pressure ratio further increases and becomes positive, a shear flow type of zero at the stagnation point is eventually realized for a pressure ratio value of approximately 2. The streamlines for this case are shown in Fig. 13b.

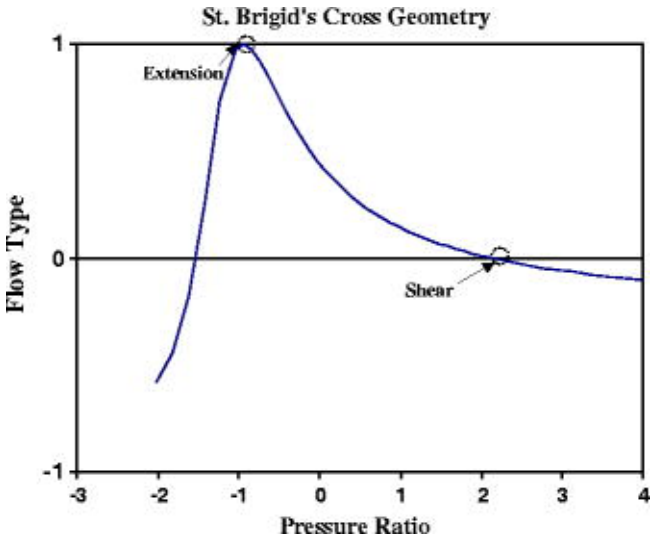

Fig. 11 Flow type (Ξ) as a function of the pressure ratio for the parallel, laterally offset, channel geometry, with side channels ("St. Brigid's Cross" geometry). The *circled points* represent the cases of extensional and shear flow, respectively

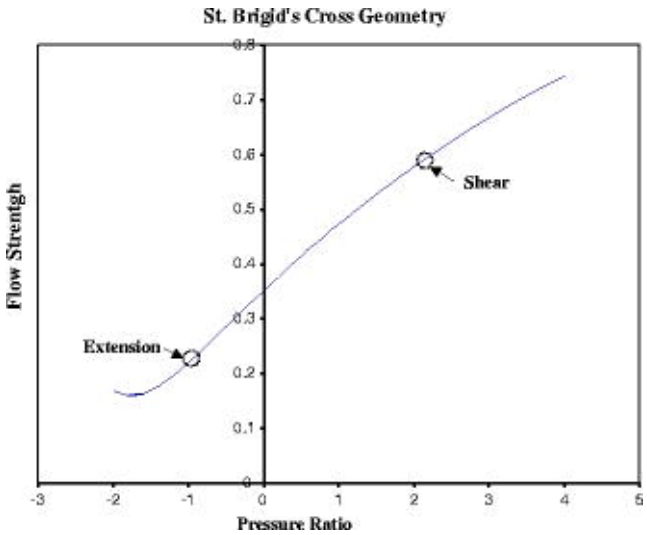

Fig. 12 Relative flow strength (S_r) as a function of the pressure ratio for the parallel, laterally offset, channel geometry, with side channels ("St. Brigid's Cross" geometry). The *circled points* represent the cases of extensional and shear flow, respectively.

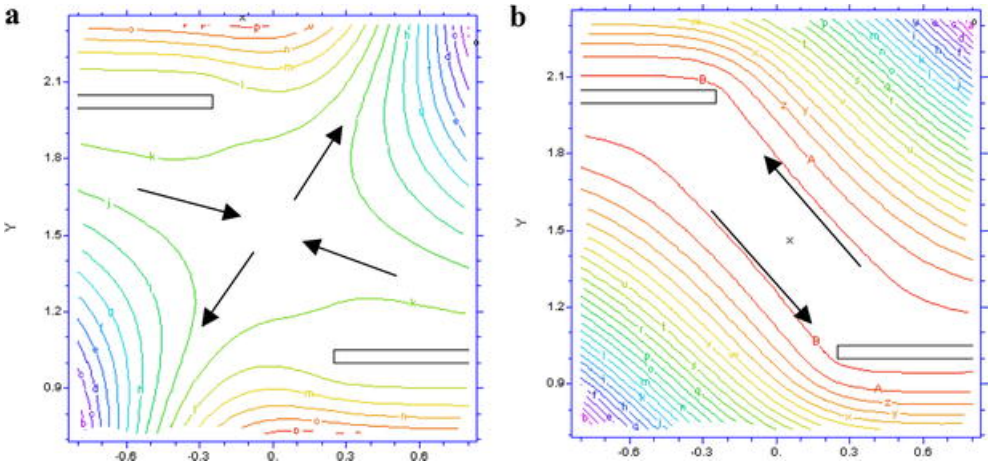

Fig. 13 Streamlines in the stagnation region for the parallel, laterally offset, channel geometry, with side channels ("St. Brigid's Cross" geometry), for the cases of **a** extension, and **b** shear

---

The relative flow strength depicted in Fig. 12 is taken relative to the average flow strength at the inlet of the flow. The plot shows that the flow strength continually rises (almost linearly) with increase in the pressure ratio. Thus, this value is higher for the case of shear than it is for extension. These values are given in Table 6. Both the extensional value of 0.23 and the shear value of 0.6, are in the acceptable range, but geometry optimization may allow better results to be achieved.

[Table 6 will appear here. See end of document.]

Flow type contour maps for the respective cases of extension and shear are shown in Figs. 14a-b. Overall, the results are somewhat comparable to the case of the laterally offset jets without the transverse flow channels. Because the fin positions are fixed in this model, and were chosen to be more favorable to shear, the flow type contours for the case of extension (Fig. 14a) have a slightly different shape than previously seen. Nevertheless, the extensional region is quite large and uniform. The shear region is also acceptably uniform, and in fact, shows better characteristics than for the original case without the transverse flow arms.

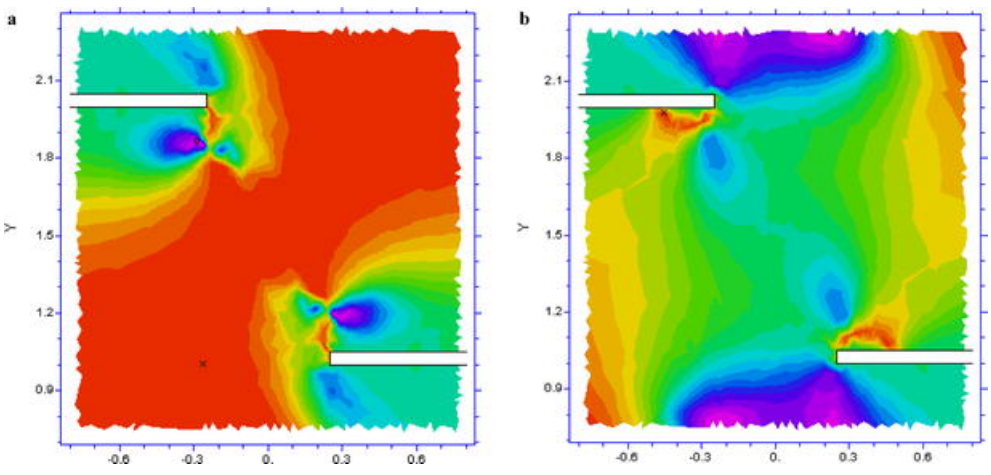

Fig. 14 Flow type (Ξ) contours in the stagnation region for the parallel, laterally offset, channel geometry, with side channels ("St. Brigid's Cross" geometry), for the cases of **a** extension, and **b** shear

The results presented here, thus far, have considered the system to be 2-D in nature. To evaluate the effect of the no-slip condition present on the walls in the third-direction on the desired flow kinematics in the stagnation region, 3-D flow simulation for varying values of the third-direction thickness (W) were undertaken. These results are shown in Fig. 15, which plots flow type versus P_{rat} along the half-plane of the device, for various values of the aspect ratio, $A=W/H_1$. The corresponding 2-D case is also plotted. The figure shows that when the aspect ratio is small. e.g., A=0.5, the flow type deviates sharply from the 2-D case, with the tendency being that the flow is much more extensional in nature, and the ability to generate shear and rotational type flows are vastly decreased (Hudson et al. 2004). However, as the aspect ratio increases, the curve gradually converges to the 2-D result, and the 2-D and 3-D results are virtually identical by about an aspect ratio of 3.

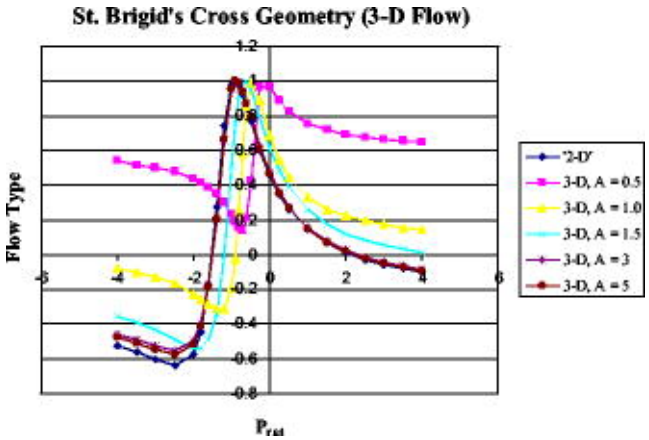

Fig. 15 Flow type (Ξ) in the half-plane versus. pressure ratio, as a function of the 3-D aspect ratio for the parallel, laterally offset, channel geometry, with side channels ("St. Brigid's Cross" geometry). The 2-D result is illustrated as well. The 3-D result converges to the 2-D case at about an aspect ratio of 3. At low aspect ratios, rotational and shear type flows are suppressed

Discussion

In developing a microfluidic device for liquid state materials characterization, the basic need is to have a suitable flow geometry for deforming the fluid in a controlled manner. Ideally, such a geometry would be able to supply a full range of linear flows in which the velocity gradient tensor is constant and the flow type is uniform. Since in practice, linear flows are not perfectly achievable,

we have sought to investigate classes of channel flows in which the full range of linear flows can be approximated in the neighborhood surrounding a stagnation point. The long fluid residence time surrounding a stagnation flow region provides a stable environment for material observation and measurement, and allows us to ignore the inhomogeneities present in complex flows, provided that the stagnation region flow gradients can be made suitably uniform.

Using a combination of finite element simulation and flow classification theory, two classes of flow geometries that fit the above criteria have been discovered. The first geometry class is based on the concept of laterally offset, opposing fluid streams. Two cases were shown based on this concept, and both were able to produce the full range of linear flow kinematics at the stagnation point, with varying, but in all cases acceptable degrees of flow strength. The results for the laterally offset channels also show that the biggest challenge in these types of flows is producing an acceptable shear field. In both the first and second geometry classes that were investigated here, shear is produced as an intermediate state in a transition from full extension to full rotation. Thus, the shear field is part of a highly elongated, almost degenerate, vortex structure, in which rotation is concentrated at the tips the vortex. The intermediate parts of the field have parallel streamlines, and a flow type very close to the desired value of zero. The key here is to minimize the effect of the rotational tips by optimizing the geometry so that the degree of rotation is weak, and to elongate the structure as much as possible to lower the flow type gradients.

This first class of geometries illustrates that the full range of the desired flow kinematics can be produced. However, they are not ideal as a microfluidics platform since they require the geometry to change to produce different flow fields. Nevertheless, they might find application in one of two ways. First, a cell could be constructed with a number of discrete geometries on it, each of which corresponds to specific desired kinematics. Such a device could operate with either a gating system that controlled which geometry was fed, or by feeding all of them simultaneously while performing the corresponding measurements. A second possibility would have to be based on some limited geometric movement in the flow device. This creates a more difficult implementation problem, but it is certainly not excluded. For example, the asymmetric cross cell could be constructed from two halves which slide one over the other in a limited way to produce the desired offset. The parallel, laterally offset, channel geometry could be employed with fins that slide to a limited degree, allowing change of the offset distance between the fin tips to change the kinematics.

The second class of flow geometries (St. Brigid's Cross) was derived based on the results of the first class. It was reasoned that if the kinematics of laterally offset fluid streams could be manipulated using geometric changes, the same effect might be obtained by simply adding additional

fluid streams normal to the existing flow directions and controlling the flow through the boundary conditions applied to the inlets and outlets of the flow. The results show that the additional transverse streams do indeed allow control of the kinematics in the stagnation region in much the same way as changing the geometry did in the previous cases studied. The full range of linear flow kinematics were produced at the stagnation point, with an acceptable degree of flow strength and uniformity. Since it is far easier to construct a device in which the flow is controlled through the boundary conditions applied to the input and output streams (rather than by mechanical movement of the flow geometry itself), this class of flow geometries is the more useful of the two we have studied. We have taken a limited look at the effect of 3-D flow in this geometry, and found that provided the aspect ratio of thickness to gap width is high enough, we can expect the 2-D flow field to be produced.

There are a number of other items that will also need to be examined in future work. The first is geometry optimization. In the results presented, complete optimization of the flow geometry parameters has not been attempted for a number of reasons. First, our primary goal in this initial study was to identify classes of geometries together with boundary condition combinations that allow us to achieve the basic goal of generating a full range of flow types. Second, such optimization needs to involve feedback from experimental work, that will allow us to discriminate between scenarios that are theoretically perfect but impossible to build, and results which are readily implemented. However, preliminary results (available as supplementary material) show that such attempts at optimization are bound to have beneficial results, and this is part of our planned future work.

Another effect that is bound to be important is non-Newtonian flow behavior when working with polymers or suspensions. For example, different types of non-Newtonian rheology (e.g., shear-thinning) might change the characteristics of the way the flow transit from extension to shear, or the conditions under which such a transition occurs. Viscoelastic effects at high Weissenburg numbers might completely alter the flow field from that observed for the Newtonian case (Groisman et al. 2003).

Summary and conclusions

In this study, the fluid dynamics of pressure driven flow in microchannels was studied for designing of a microfluidic, liquid state, materials characterization device. Classes of channel flows in which a full range of linear flows could be approximated in the neighborhood surrounding a stagnation

point were investigated by means of finite element flow simulations, together with flow classification criteria. Two classes of flow geometries were identified in which the flow type can be adjusted between shear and extension in the neighborhood surrounding the stagnation point, while providing adequate flow strength. A key feature, inherent to both is that they make use of opposing, laterally offset fluid streams. The opposing fluid streams are necessary to produce a stagnation point, and the lateral offset is necessary in order to generate vorticity and produce mixed flows at the stagnation point (including shear). In the first geometry class, the flow type is manipulated by changing parameters inherent to the base geometry. This first case was used as a baseline for identifying a second class in which the flow type can be manipulated by varying the pressure boundary conditions while keeping the geometry constant. The latter case is the more useful both in terms of ease of implementation and of experimental design and control.

References

FIDAP (2003a) Users Manual. Fluent, Evanston

FlexPDE (2003b) Users Manual. PDE Solutions

Astarita G (1979) Objective and generally applicable criteria for flow classification. J Non-Newton Fluid Mech 6:69–76

Bentley BJ, Leal GL (1986a) A computer controlled four-roll mill for investigations of particle and drop dynamics in two-dimensional linear shear flows. J Fluid Mech 167:219–240

Bentley BJ, Leal GL (1986b) An experimental investigation of drop deformation and breakup in steady, two-dimensional flows. J Fluid Mechs 167:241–283

Berry MV, Mackley MR (1977) The six roll mill - unfolding an unstable persistently extensional flow. Philos Trans R Soc Lond Ser A-Math Phys Eng Sci 287:1–16

Bird B, Armstrong RA, Hassager O (1982) Dynamics of Polymeric Liquids. Wiley, Newyork

Ceriotti L, Weible K, de Rooij NF, Verpoorte E (2003) Rectangular channels for lab-on-a-chip applications. Microelectr Eng 67–8:865–871

Chella R, Ottino JM (1985) Stretching in some classes of fluid motions and asymptotic mixing efficiencies as a measure of flow classification. Arch Ration Mech Anal 90:15–42

Chow A, Keller A, Muller AJ, Odell JA (1988) Entanglements in polymer-solutions under elongational flow—a combined study of chain stretching, flow velocimetry, and elongational viscosity. Macromolecules 21:250–256

Chow AW (2002) Lab-on-a-chip: opportunities for chemical engineering. Aiche J 48:1590–1595

De Gennes PG (1974) Coil-stretch transition of dilute flexible polymers under ultrahigh velocity gradients. J Chem Phys 60:5030–5042

Frank FC, Mackley MR (1976) Localized flow birefringence of polyethylene oxide solutions in a two roll mill. J Polym Sci A 214:1121–1131

Fuller GG, Leal LG (1981) Flow birefringence of concentrated polymer-solutions in two-dimensional flows. J Polym Sci Part B-Polym Phys 19:557–587

Groisman A, Enzelberger M, Quake SR (2003) Microfluidic memory and control devices. Science 300:955–958

Hasselbrink EF, Shepodd TJ, Rehm JE (2002) High-pressure microfluidic control in lab-on-a-chip devices using mobile polymer monoliths. Anal Chem 74:4913–4918

Higdon JJL (1993) The kinematics of the 4-roll mill. physics of fluids a-fluid dynamics 5:274–276

Hills CP (2002) Flow patterns in a two-roll mill. Q J Mech App Math 55:273–296

Hudson SD, Phelan FR Jr, Handler MD, Cabral JT, Migler KB, Amis EJ (2004) Microfluidic analog of the four-roll mill. Appl Phys Lett 85(2):335–337

Huilgol RR (1980) Comments on objective and generally applicable criteria for flow classification. J Non-Newton Fluid Mech 7:91–95

Keller A, Odell JA (1985) The extensibility of macromolecules in solution—a new focus for macromolecular science. Colloid Polym Sci 263:181–201

Lee ICY, Kapur N, Gaskell PH, Savage MD, Homsy GM (2002) Birefringent strands in polymer flows in a co-rotating two-roll mill. J Non-Newton Fluid Mech 104:33–51

Ouellette J (2003) A new wave of microfluidic devices. August–September:14–17

Price TJ, Mullin T, Kobine JJ (2003) Numerical and experimental characterization of a family of two-roll-mill flows. Proc R Soc Lond Ser A Math Phys Eng Sci 459:117–135

Remmelgas J, Leal LG (2000) Computational studies of the FENE-CR model in a two-roll mill. J Non-Newton Fluid Mech 89:231–249

Reyes MAH, Geffroy E (2000a) A corotating two-roll mill for studies of two-dimensional elongational flows with vorticity. Phys Fluids 12:2372–2376

Reyes MAH, Geffroy E (2000b) Study of low Reynolds number hydrodynamics generated by symmetric co-rotating two-roll mills. Rev Mex Fis 46:135–147

Singh P, Leal LG (1996) Computational studies of the FENE dumbbell model with conformation-dependent friction in a co-rotating two-roll mill. J Non-Newton Fluid Mech 67:137–178

Tanner RI (1976) Test Particle Approach to Flow Classification for Viscoelastic Fluids. Aiche Journal 22:910–918

Taylor GI (1934) The formation of emulsions in definable fields of flow. Proc R Soc Lond Ser A-Math Phys Eng Sci 146:501–523

Thompson RL, Mendes PRS (2004) Persistence of straining and flow classification. Int J Eng Sci (accepted)

Thorsen T, Maerkl SJ, Quake SR (2002) Microfluidic large-scale integration. Science 298:580–584

Table 1 Geometry parameters and boundary conditions used for the asymmetric cross flow cell

Channel width (H)	Channel length (L)	Inlet pressure (P_{in})	Outlet pressure (P_{out})
1	7	1	0

Table 2 Values for flow type and flow strength at the stagnation point for the asymmetric cross flow cell at offset distances mostly closely corresponding to the cases of extension, shear and rotation

Case	Offset distance (d_{off})	Flow type	Relative flow strength
Extension	0	0.9995	2.35
Shear	1.5	−0.0141	0.25
Rotation	2	−0.9075	0.024

Table 3 Geometry parameters and boundary conditions used for the parallel, laterally offset, channels

Inlet width (h)	Outlet width (H)	Fin width (H_{fin})	Channel length (L)	Inlet pressure (P_{in})	Outlet pressure (P_{out})
1	2	0.05	5	1	0

Table 4 Values for flow type and flow strength at the stagnation point for the parallel, laterally offset, channels at offset distances mostly closely corresponding to the cases of extension, shear and rotation

Case	Offset distance (d)	Flow type	Relative flow strength
Extension	3.2	0.996	0.452
Shear	0.5	−0.004	0.414
Rotation	−0.14	−0.989	0.01

Table 5 Geometry parameters and boundary conditions used for the parallel, laterally offset, channel geometry, with side channels ("St. Brigid's Cross" geometry)

Inlet width (H_{in})	Inlet/outlet width 1 (H_1)	Inlet/outlet width 2 (H_2)	Fin width (H_{fin})	Channel length (L)	Offset distance	Pressure magnitude (P_{mag})	Inlet pressure (P_{in})
2	1	2	0.05	5	0.5	1.0	0

Table 6 Values for flow type and flow strength at the stagnation point for the parallel, laterally offset, channel geometry, with side channels ("St. Brigid's Cross" geometry), at offset distances mostly closely corresponding to the cases of extension and shear

Case	Pressure ratio (P_{rat})	Pressure 1 (P_1)	Pressure 2 (P_2)	Flow type	Relative flow strength
Extension	−0.9	0.9	−1	0.9995	0.233
Shear	2.2	2.2	−1	−0.0044	0.596